Robust Suboptimal Recursive Least-Squares Fixed-Lag Smoothing Technique with Polynomial/ Fourier Series Approximations of Covariance Information for Linear Continuous-Time Stochastic Systems with Uncertainties

SEIICHI NAKAMORI
Professor Emeritus, Faculty of Education,
Kagoshima University,
1-20-6, Korimoto, Kagoshima, 890-0065,
JAPAN

Abstract: - The dual use of covariance information enables filtering and smoothing algorithms to effectively capture statistical dependencies and mitigate the effects of system uncertainties and observation noise. In the fixed-point smoother and filter, the existing literature approximates covariance information using finite Fourier series expansions. Building upon this foundation, the present work originally introduces a newly designed robust recursive least-squares fixed-lag (FL) smoother tailored for linear continuous-time stochastic systems with uncertainties. In this framework, the autocovariance function of the degraded signal is modeled as a semi-degenerate function, while the cross-covariance function between the signal and the observed measurements is represented as a degenerate function. This paper emphasizes approximating both covariance structures using polynomials and finite Fourier series, thereby enabling flexible, computationally efficient modeling of statistical dependencies essential for robust state estimation. As demonstrated in the numerical simulation example, the mean-square values (MSVs) of the approximation errors associated with both the autocovariance and cross-covariance functions are negligible, indicating high fidelity in the modeling process. Based on polynomial approximations, the estimation accuracy of both the robust filter and the FL smoother is evaluated, highlighting their effectiveness in capturing key statistical dependencies. Additionally, the simulation includes a comparative example in which signal estimation is performed using covariance data approximated via finite Fourier series expansions. The results indicate that both the polynomial- and Fourier-based approximations strategies reliably and consistently support the robustness of the proposed estimation framework.

Key-Words: - Robust RLS fixed-lag smoother, stochastic systems with uncertainties, continuous-time stochastic systems, covariance information, polynomial approximation, finite Fourier series expansion.

Received: August 16, 2025. Revised: October 29, 2025. Accepted: March 11, 2026. Published: June 10, 2026.

1 Introduction

This study examines fixed-lag (FL) smoothing problems within uncertain continuous-time stochastic systems. Previous research [1] explored advancements in state estimation by applying an extended Kalman filter in conjunction with a FL smoother. The results demonstrated improved estimation performance, especially in the presence of model inaccuracies and measurement noise. These outcomes emphasize the significance of FL smoothing methods for enhancing estimation robustness and accuracy in practical system environments. Specifically, it emphasizes the enhanced estimation capabilities offered by the smoother in model errors and measurement noise. In [2], the researchers proposed an efficient method for simultaneously estimating inputs and states in vibrating structures. Their approach integrates an extended Kalman filter with a FL smoother to achieve this goal. The article in [3] details the new achievements and significance of FL smoothing algorithms in mobile robot motion tracking. The proposed method demonstrates excellent accuracy, particularly in complex environments, greatly expanding its potential for future research and implementation. Reference [4] improves estimation accuracy and computational efficiency in linear discrete-time time-varying state-space models by introducing an unbiased minimum-variance receding-horizon FL smoother. Numerical experiments validate the theoretical reliability of this method. Reference [5] suggests a new approach to

FL smoothing in Markov transition systems that greatly improves estimation accuracy. This study evaluates algorithms based on the interacting multiple model (IMM) approach, detailing their respective strengths and limitations. Reference [6] addresses the finite-horizon H_∞ FL smoothing problem for linear descriptor systems, introducing a new method that uses Kronecker space to handle delayed measurements. Reference [7] introduces a new approach to FL smoothing involving linear equality constraints and illustrates how the performance of the proposed algorithm can be improved. Applying state augmentation is a promising strategy for solving complex problems. The study in [8] demonstrates the evolution from conventional methods by detailing the importance and advantages of the FL maximum likelihood smoother. The study in [9] emphasizes the importance of a distributed Kalman smoother based on the optimal fusion criterion for integrating data in complex sensor systems. [10] presents a novel approach to distributed Kalman filtering and smoothing and explores its practical applications. The authors demonstrated that sharing information between nodes via the proposed diffusion strategy improved the overall system performance. The study presented in [11] proposes a novel robust estimation framework that advances beyond traditional methodologies by introducing a receding horizon (RH) FL smoother specifically designed for systems with bounded uncertainties. The proposed approach minimises maximum estimation error by using set-valued state estimation techniques and representing uncertainty with ellipsoidal bounds. This formulation rigorously captures the worst-case estimation error, enhancing the reliability of the smoothing algorithm under uncertain and noisy conditions. Researchers proposed a computationally efficient FL smoother in [12], and its effectiveness was verified. This smoother has the potential to provide reliable estimates while reducing the computational load and can be useful for various applications. Furthermore, its practicality is enhanced by providing guidelines for selecting the window length. Reference [13] proposes a computationally efficient FL smoother and verifies its effectiveness. This smoother provides reliable estimates while reducing the computational load, thereby increasing its applicability. Furthermore, the inclusion of guidelines for selecting the window length enhances its practical applicability. The article [14] introduced a robust FL smoother for nonlinear uncertain systems. It proposes a unified approach that combines a nonlinear robust estimator with a stable FL smoother to improve the estimation error covariance. The study in [15] emphasizes the significance of structural health monitoring and introduces a novel estimation method. Approaches capable of accurately estimating structural responses from noisy or limited data are essential for ensuring structural safety.

The author proposed a recursive least-squares FL smoothing algorithm using covariance information in linear stochastic systems [16]. The semi-degenerate function represents the autocovariance function of the signal. In [17], the authors presented a semi-degenerate kernel formulation for a Fredholm integral equation. Some manipulations convert the Fredholm integral equation into an initial-value system. Finite Fourier series expansions approximate the autocovariance and cross-covariance functions from their data [16]. Methods employing covariance information are mutually alternative to estimation techniques using state-space models in robust estimation problems. This approach does not utilise all the information contained within the state-space model. This study examines the development of a robust suboptimal recursive FL smoothing technique for linear continuous-time stochastic systems with uncertainties. The semi-degenerate function represents the autocovariance of the degraded signal. If the cross-covariance function takes a semi-degenerate form, it is difficult to derive the robust recursive least-squares FL smoothing algorithm. The explanation lies in the fact that the cross-covariance function does not exhibit even function properties. To overcome this drawback, this paper employs a degenerate kernel function to express the cross-covariance function between the signal and the degraded observation. It is necessary to approximate the covariance information in functional forms. For this purpose, this paper employs polynomial approximations in addition to finite Fourier series expansions to approximate autocovariance and cross-covariance data functionally. Several polynomial approximation methods are explored, including piecewise linear [18] and quadratic/cubic spline interpolation [18], as well as the least-squares (LS) method for fitting an appropriate-order polynomial function to data [19], [20], [21]. [19] and [20] utilize the MATLAB function polyfit.m for polynomial curve fitting. It estimates the coefficients of a polynomial that best fits a given set of data in the LS sense. The function requires input vectors representing the horizontal (independent) and vertical (dependent) axis data, along with the desired degree of the polynomial. Upon execution, polyfit.m returns a vector of coefficients corresponding to the fitted polynomial.

Section 2 introduces the state-space models for the signal and its degraded system, with the latter featuring uncertain parameters in its observation vector and system matrix. Section 3 introduces a robust FL smoothing problem in linear LS estimation with covariance information. Theorem 1 in Section 4 presents the robust RLS-FL smoothing algorithm. Section 5 details the use of polynomial approximations to model the cross-covariance between the signal and the observed measurements, as well as the autocovariance of the degraded signal. With these approximations, an efficient representation of covariance structures is possible, which is key for robust estimation. Section 6 introduces an alternative approach using finite Fourier series expansions to approximate both the autocovariance of the degraded signal and the cross-covariance between the signal and observations. Section 7 provides a numerical simulation example of the robust FL smoother using the polynomial / finite Fourier series approximations of the covariance data. This approach further demonstrates the effectiveness of both modeling techniques for robust state estimation. author introduced the robust fixed-point smoother and filter using the covariance information in linear continuous-time stochastic systems with uncertainties

2 Original State-Space Model and Degraded State-space Model with Uncertainties

Consider a state-space model (1) that satisfies the observability condition for linear continuous-time stochastic systems.

$$\begin{aligned}
&y(t) = z(t) + v(t), z(t) = Hx(t),\\
&\frac{dx(t)}{dt} = Ax(t) + \Gamma w(t), x(0) = c,\\
&E[v(t)v(s)] = R\delta(t-s),\\
&E[w(t)w^T(s)] = Q\delta(t-s),\\
&E[v(t)w^T(s)] = 0, E[x(0)w^T(t)] = 0,\\
&E[x(0)v(t)] = 0, 0 \le \mathrm{s}, \mathrm{t}
\end{aligned} \tag{1}$$

$x(t) \in R^n$ is the state, and $z(t)$ is the signal that has to be estimated. The input noise $w(t) \in R^l$ and the observation noise $v(t)$ are zero-mean, white, Gaussian, and uncorrelated. Γ is the $n \times l$ input matrix, and H is the $1 \times n$ observation vector. In (1), the autocovariance functions of the observation noise $v(t)$ and the input noise $w(t)$ are both described using the Dirac delta function. This paper examines state and observation equations that incorporate uncertain parameters within a state-space model.

$$\begin{aligned}
&\breve{y}(t) = \breve{z}(t) + v(t),\\
&\breve{z}(t) = \overleftrightarrow{H}(t)\overleftrightarrow{x}(t), \overleftrightarrow{H}(t) = H + \Delta H(t),\\
&\frac{d\overleftrightarrow{x}(t)}{dt} = \overleftrightarrow{A}(t)\overleftrightarrow{x}(t) + \Gamma w(t),\\
&\overleftrightarrow{A}(t) = A + \Delta \mathrm{A}(t),\\
&\mathrm{E}[\Delta A(\mathrm{t})w^T(\mathrm{s})] = 0,\\
&E[\Delta H(t)v(s)] = 0, E[\overleftrightarrow{x}(0)w^T(t)] = 0,\\
&E[\overleftrightarrow{x}(0)v(t)] = 0,\ 0 \le \mathrm{s}, \mathrm{t}
\end{aligned} \tag{2}$$

In (2), the system matrix A and observation vector H are replaced by their time-varying degraded counterparts, A and H. The elements of $\Delta A(t)$ and the components of $\Delta H(t)$ represent uncertain variables. The initial state vector $\acute{x}(0)$ is generated randomly and remains independent of both the input and measurement noise.

3 Robust LS-FL Smoothing Problem

Let the FL smoothing estimate $\hat{z}(t-Lag, t)$ of the signal $z(t-Lag)$ be denoted by

$$\hat{z}(t-Lag, t) = \int_0^t h(t,s)\breve{y}(s)ds, \tag{3}$$

where $\breve{y}(s)$ represents the observed value for $0 \le s \le t$ and $h(t,s)$ is the impulse response function. The main goal is to minimize the mean-square value

$$J = E[(z(t-Lag) - \hat{z}(t-Lag,t))^2] \tag{4}$$

of the FL smoothing errors, $z(t-Lag) - \hat{z}(t-Lag,t)$. According to the orthogonal projection lemma

$$z(t-Lag) - \hat{z}(t-Lag,t) \perp \breve{y}(s), \tag{5}$$

the FL smoothing estimate $\hat{z}(t-Lag,t)$ minimizes the cost function J. In this framework, the optimal impulse response function is characterized by the Wiener–Hopf integral equation

$$\begin{aligned}
&E[z(t-Lag)\breve{y}^T(s)] =\\
&\int_0^t h(t,\tau)E[\breve{y}(\tau)\breve{y}^T(s)]ds,
\end{aligned} \tag{6}$$

which provides the necessary condition for minimizing the mean-square estimation errors. Substituting the degraded observation (2) into (6) yields a Volterra integral equation of the second kind (7).

$$\begin{aligned}
&h(t,s)R\\
&= K_{z\breve{y}}(t-Lag,s)\\
&- \int_0^t h(t,\tau)K_{\breve{z}}(\tau,s)d\tau, K_{z\breve{y}}(t,s)\\
&= E[z(t)\breve{y}^T(s)],\\
&K_{\breve{z}}(t,s) = E[\breve{z}(t)\breve{z}^T(s)]
\end{aligned} \tag{7}$$

$K_{z\check{y}}(t,s)$ is the cross-covariance function of the signal $z(t)$ with the degraded observed value $\check{y}(s)$. The cross-covariance function $K_{z\check{y}}(t,s)$ assumes the form of a degenerate kernel, which is independent of the relative magnitudes of t and s. This structural property simplifies the representation of statistical dependencies between the signal and the degraded observations, as the kernel can be expressed in terms of separable functions rather than requiring explicit dependence on the ordering of the time variables. Such a formulation not only reduces analytical complexity but also facilitates the tractable construction of robust FL smoothing estimators.

$$K_{z\check{y}}(t,s) = \alpha(t)\beta^T(s) \tag{8}$$

$K_{\check{z}}(t,s)$ is the autocovariance function of the degraded signal $\check{z}(t)$, expressed by (9) in the semi-degenerate kernel form [16].

$$K_{\check{z}}(t,s) = \begin{cases} \check{A}(t)\check{B}^T(s), 0 \le s \le t, \\ \check{B}(t)\check{A}^T(s), 0 \le t \le s \end{cases} \tag{9}$$

Wide-sense stationary stochastic systems allow the representation of $K_{z\check{y}}(t,s)$ and $K_{\check{z}}(t,s)$ as $K_{z\check{y}}(\tau)$ and $K_{\check{z}}(\tau)$, respectively, with $\tau = t - s$. $K_{\check{z}}(\tau)$ is an even function of τ. This paper employs approximations using both polynomials and Fourier series for $K_{\check{z}}(\tau)$ and $K_{z\check{y}}(\tau)$. The semi-degenerate function represents the autocovariance of the degraded signal. If the cross-covariance function takes a semi-degenerate form, it is difficult to derive the robust recursive least-squares FL smoothing algorithm. The explanation lies in the fact that the cross-covariance function does not exhibit even function properties. To overcome this drawback, this paper employs a degenerate kernel function to express the cross-covariance function between the signal and the degraded observation.

4 Robust RLS-FL Smoothing Algorithm

Given the covariance functions $K_{z\check{y}}(t,s)$ and $K_{\check{z}}(t,s)$ defined in (8) and (9), Theorem 1 presents the robust RLS-FL smoothing algorithm for the signal. From the Volterra integral equation (7), Theorem 1 is derived based on the invariant imbedding method [16], [17]. The invariant imbedding method transforms the Volterra integral equation into an initial-value system for the robust RLS-FL smoothing algorithm, as proposed in Theorem 1. The derivation steps are proved in detail in a mathematically rigorous manner.

Theorem 1 Let (1) define the state-space model for the true signal z(t), and let (2) describe the state-space model for the degraded signal $\check{z}(t)$. The cross-covariance function $K_{z\check{y}}(t,s)$ between the signal z(t) and the observed measurement $\check{y}(s)$ is given by (8), while the autocovariance function $K_{\check{z}}(t,s)$ of the degraded signal $\check{z}(t)$ is defined in (9). Equations (10) through (16) collectively form the initial-value system for calculating the robust RLS-FL smoothing estimate $\hat{z}(t-Lag,t)$ of the signal $z(t-Lag)$, based on the degraded observations $\check{y}(t)$ described in (2).

FL smoothing estimate of the signal $z(t-Lag)$: $\hat{z}(t-Lag,t)$

$$\hat{z}(t-Lag,t) = \alpha(t-Lag)e(t) \tag{10}$$

Differential equations for $e(t)$:

$$\frac{de(t)}{dt} = J(t,t)(\check{y}(t) - \check{A}(t)e_1(t)), e(0)=0 \tag{11}$$

Differential equations for $e_1(t)$:

$$\frac{de_1(t)}{dt} = J_1(t,t)(\check{y}(t) - \check{A}(t)e_1(t)), \quad e_1(0) = 0 \tag{12}$$

Equation for $J(t,t)$:

$$J(t,t) = (\beta^T(t) - r(t)\check{A}^T(t))/R \tag{13}$$

Equation for $J_1(t,t)$:

$$J_1(t,t) = (\check{B}^T(t) - r_1(t)\check{A}^T(t))/R \tag{14}$$

Differential equations for $r(t)$:

$$\frac{dr(t)}{dT} = J(t,t)(\check{B}(t) - \check{A}(t)r_1(t)), \quad r(0) = 0 \tag{15}$$

Differential equations for $r_1(t)$:

$$\frac{dr_1(t)}{dt} = J_1(t,t)(\check{B}(t) - \check{A}(t)r_1(t)), \quad r_1(0) = 0 \tag{16}$$

For the asymptotic stability of the fixed-lag smoothing algorithm in Theorem 1, the following conditions are required. Specifically, for the asymptotic stability of the differential equations (12) and (15), all the real parts of the eigenvalues of $-J_1(t,t)\check{A}(t)$ must be negative.

Now, let us derive a recursive expression for the cost function J defined in (4). From (3), (8), and (A-15), J is transformed as follows:

$$J = K_z(t-Lag,t-Lag) - E[\hat{z}(t-Lag,t)z(t-Lag)]$$

$$= K_z(t-Lag,t-Lag) - \int_0^t h(t,s')z(t-Lag)\check{y}(s')ds$$
$$= K_z(t-Lag,t-Lag) - \alpha(t-Lag)\int_0^t J(t,s')K_{z\check{y}}(t,s')\check{y}(s')ds'$$
$$= K_z(t-Lag,t-Lag) - \alpha(t-Lag)\int_0^t J(t,s')\alpha(t)\beta^T(s')ds'.$$

Introducing $l(t)=\int_0^t J(t,s')\beta(s')ds'$, the above equation can be rewritten in the form given by (17).

$$J = K_z(t-Lag,t-Lag) - \alpha(t-Lag)l(t)\alpha^T(t) \quad (17)$$

Differentiating $l(t)$ with respect to t, and using (A-5), we obtain

$$\frac{dl(t)}{dt} = J(t,t)\beta(t) + \int_0^t \frac{\partial J(t,s')}{\partial t}\beta(s')ds'$$
$$= J(t,t)\beta(t) - J(t,t)\check{A}(t)\int_0^t J_1(t,s')\beta(s')ds'.$$

Introducing $p(t)=\int_0^t J_1(t,s')\beta(s')ds'$, the above equation can be rewritten in the form given by (18).

$$\frac{dl(t)}{dt} = J(t,t) \times(\beta(t)-\check{A}(t)p(t)) \quad l(0)=0 \quad (18)$$

Differentiating $p(t)$ with respect to t, and using (A-13), we obtain (19).

$$\begin{aligned}\frac{dp(t)}{dt} &= J_1(t,t)\beta(t) + \int_0^t \frac{\partial J_1(t,s')}{\partial t}\beta(s')ds'\\ &= J_1(t,t)\beta(t) - J_1(t,t)\check{A}(t)\int_0^t J_1(t,s')\beta(s')ds'\\ &= J_1(t,t)(\beta(t)-\check{A}(t)p(t)),\\ p(0)&=0\end{aligned} \quad (19)$$

Hence, the cost function is calculated recursively using (13), (14), (15), (16), (17), (18), and (19). The cost function can be rewritten as
$J = K_z(t-Lag,t-Lag) - E[\hat{z}(t-Lag,t)^2]$.
From this equation, the variance of the FL smoothing estimate is upper and lower bounded as
$0 \le E[\hat{z}(t-Lag,t)^2] \le K_z(t-Lag,t-Lag)$.

This demonstrates the existence of an asymptotically stable FL smoother.

Refer to the Appendix for the proof of Theorem 1.

In the FL smoothing framework, the cross-covariance function $K_{z\check{y}}(t,s)$ is represented in degenerate kernel form. Notably, the integral equation (7) incorporates the term $K_{z\check{y}}(t-Lag,s)$, which plays a central role in the smoothing estimate. The degenerate kernel formulation of $K_{z\check{y}}(t,s)$, as defined in (8), facilitates the analytical expansion of the integral equation, enabling tractable computation. Besides the Fourier series expansion to be introduced in Section 6, this paper also employs polynomial approximations in Section 5 for both $K_{z\check{y}}(t,s)$ and the autocovariance function $K_{\check{z}}(t,s)$. This enhances both the flexibility and computational efficiency of modeling the covariance structure.

5 Polynomial Approximations of Autocovariance Data of Degraded Signal and Cross-Covariance Data between Signal and Degraded Observation

Let $K_{\check{z}}(\tau)$, where $\tau=t-s$, denote the autocovariance function $K_{\check{z}}(t,s)$ of the degraded signal $\check{z}(t)$ in wide-sense stationary stochastic systems. Due to stationarity, $K_{\check{z}}(\tau)$ depends solely on the time difference τ and is an even function, satisfying $K_{\check{z}}(\tau)=K_{\check{z}}(-\tau)$. To facilitate analytical and numerical treatment, a finite-order polynomial expansion as defined in (20) is employed to approximate $K_{\check{z}}(\tau)$. The resulting approximation, denoted $\hat{K}_{\check{z}}(\tau)$, consists of $k+1$ terms and provides a tractable representation of the autocovariance function suitable for integration into the robust FL smoothing framework.

$$\begin{aligned}\hat{K}_{\check{z}}(\tau) &= P_1\tau^k + P_2\tau^{k-1} + \cdots + P_{k-1}\tau^2 + P_k\tau + P_{k+1}\\ &= P_1(t-s)^k + P_2(t-s)^{k-1} + \cdots + P_{k-1}(t-s)^2 + P_k(t-s) + P_{k+1},\\ & 0\le\tau\le D\end{aligned} \quad (20)$$

The polynomial fitting approximates $K_{\check{z}}(\tau)$ by $\hat{K}_{\check{z}}(\tau)$ based on linear-least squares approximation method minimizing the sum of the squares of the approximation errors $K_{\check{z}}(\tau)-\hat{K}_{\check{z}}(\tau)$ for $0\le\tau\le D$. The comparison between the autocovariance function $K_{\check{z}}(t,s)$ in (9) and its polynomial approximation in (17) reveals the underlying structure of the K-dimensional vector components of $\check{A}(t)$ and $\check{B}(t)$. From (9), $K_{\check{z}}(t,s)$ for $0\le s\le t$ is expressed as $\check{A}(t)\check{B}^T(s)$, and $K_{\check{z}}(t,s)$ for $0\le t\le s$ is expressed as $K_{\breve{z}}(t,s) = \breve{B}(t)\breve{A}^T(s)$. From this consideration, we can get an even function $\hat{K}_{\breve{z}}(\tau)$ of $K_{\breve{z}}(\tau)$ for $-D \le \tau \le D$, approximately . The following components arise naturally when (20) is expanded with respect to t and s.

$$\breve{A}(t) = \begin{bmatrix}\breve{A}_1(t) & \breve{A}_2(t) & \breve{A}_3(t) & \cdots & \breve{A}_K(t)\end{bmatrix}$$
$$\breve{B}(t) = \begin{bmatrix}\breve{B}_1(t) & \breve{B}_2(t) & \breve{B}_3(t) & \cdots & \breve{B}_K(t)\end{bmatrix}$$

In wide-sense stationary stochastic systems, the cross-covariance function $K_{z\breve{y}}(t,s)$ between the signal $z(t)$ and the observed measurement $\breve{y}(s)$, depends solely on the time difference $\tau = t - s$, and is thus denoted as $K_{z\breve{y}}(\tau)$. (21) introduces a finite-order polynomial approximation of this function, enabling tractable analytical and numerical treatment. The approximated function, denoted $\hat{K}_{z\breve{y}}(\tau)$, consists of $m+1$ terms and serves as a compact representation of the cross-covariance structure, facilitating its integration into the robust FL smoothing framework.

$$\begin{aligned}\hat{K}_{z\breve{y}}(\tau) &= D_1\tau^m + D_2\tau^{m-1} + \cdots \\ &+D_{m-1}\tau^2 + D_m\tau + D_{m+1} \\ &= D_1(t-s)^m + D_2(t-s)^{m-1} \\ &+ \cdots + D_{m-1}(t-s)^2 + D_m(t-s) \\ &+D_{m+1}, -D \le \tau \le D\end{aligned} \tag{21}$$

The polynomial fitting approximates $K_{z\breve{y}}(\tau)$ by $\hat{K}_{z\breve{y}}(\tau)$ based on linear-least squares approximation method minimizing the sum of the squares of the approximation errors $K_{z\breve{y}}(\tau) - \hat{K}_{z\breve{y}}(\tau)$ for $-D \le \tau \le D$. The comparison between the autocovariance function $K_{z\breve{y}}(t,s)$ in (8) and its polynomial approximation in (21) reveals the underlying structure of the M-dimensional vector components of $\alpha(t)$ and $\beta(t)$. The following components arise naturally when (21) is expanded with respect to t and s.

$$\alpha(t) = [\alpha_1(t) \quad \alpha_2(t) \quad \alpha_3(t) \quad \cdots \quad \alpha_M(t)]$$
$$\beta(t) = [\beta_1(t) \quad \beta_2(t) \quad \beta_3(t) \quad \cdots \quad \beta_M(t)]$$

This finite-dimensional formulation simplifies the analysis of covariance structures and facilitates the systematic construction of a robust FL smoothing estimator. These components encapsulate the time-varying coefficients derived from the polynomial functions used to approximate the covariance behaviour.

The suboptimal smoothing estimate $\hat{z}(t - Lag, t)$ of the signal $z(t - Lag)$ can be recursively computed from the degraded observations $\breve{y}(t)$ by substituting the functions $\breve{A}(t)$, $\breve{B}(t)$, $\alpha(t)$, and $\beta(t)$ into the robust RLS-FL smoothing algorithm outlined in Theorem 1. This recursive formulation enables efficient implementation and real-time applicability in uncertain continuous-time stochastic systems.

6 Finite Fourier Series Approximations of Autocovariance Data of Degraded Signal and Cross-Covariance Data of Signal with Observed Value

In wide-sense stationary stochastic systems, the autocovariance function $K_{\breve{z}}(t,s)$ of the degraded signal $\breve{z}(t)$ is commonly written as $K_{\breve{z}}(\tau)$, where $\tau = t - s$. For all τ in its domain, $K_{\breve{z}}(\tau)$ is an even function. We approximate $K_{\breve{z}}(\tau)$ by a finite Fourier cosine series expansion, as shown in (22). The function $\hat{K}_{\breve{z}}(\tau)$ uses $N+1$ terms to approximate $K_{\breve{z}}(\tau)$. The Fourier components converge to zero, i.e., $a_i \to 0$ as $i \to \infty$, provided that the auto-covariance function $K_{\breve{z}}(\tau)$ is bounded (i.e., exhibits no divergences).

$$\begin{aligned}&\hat{K}_{\breve{z}}(\tau) \approx \frac{a_0}{2} + \sum_{i=1}^{N} a_i cos(i\omega_0\tau), \\ &\omega_0 = \frac{2\pi}{T}, \frac{-T}{2} \le \tau \le \frac{T}{2}\end{aligned} \tag{22}$$

Here, T represents the fundamental period of $K_{\breve{z}}(\tau)$. The finite Fourier cosine coefficients are calculated by (23).

$$\begin{aligned}&a_i = \frac{2}{T}\int_{\frac{-T}{2}}^{\frac{T}{2}} K_{\breve{z}}(\tau) cos(i\omega_0\tau) d\tau, \\ &i = 0,1,2,\cdots,N\end{aligned} \tag{23}$$

After comparing (9) and (22), we can represent the vector components of $\breve{A}(t)$ and $\breve{B}(t)$ as follows:

$\breve{A}(t) = \begin{bmatrix}\breve{A}_1(t) & \breve{A}_2(t) & \breve{A}_3(t) & \cdots & \breve{A}_{2N+1}(t)\end{bmatrix}$,
$\breve{B}(t) = \begin{bmatrix}\breve{B}_1(t) & \breve{B}_2(t) & \breve{B}_3(t) & \cdots & \breve{B}_{2N+1}(t)\end{bmatrix}$,
$\breve{A}_1(t) = \frac{a_0}{2}$,
$\breve{A}_i(t) = a_{i-1} cos(\frac{2\pi(i-1)t}{T})$, $i = 2, 3, \cdots, N+1$,
$\breve{A}_i(t) = a_{i-(N+1)} sin(\frac{2\pi(i-(N+1))t}{T})$, $i = N+2, N+3, \cdots, 2N+1$,
$\breve{B}_1(t) = 1$,
$\breve{B}_i(t) = cos(\frac{2\pi(i-1)t}{T})$, $i = 2, 3, \cdots, N+1$,
$\breve{B}_i(t) = si\,n\left(\frac{2\pi\big(i-(N+1)\big)t}{T}\right)$,
$i = N+2, N+3, \cdots, 2N+1$.

The cross-covariance function $K_{z\check{y}}(t,s)$ of $z(t)$ with $\check{y}(s)$ is given by (8). Let $K_{z\check{y}}(\tau)$ be approximated by the finite Fourier series transformations. In (24), $\hat{K}_{z\check{y}}(\tau)$ denotes the finite Fourier series expansion that approximates $K_{z\check{y}}(\tau)$ with $2J+1$ terms. The Fourier components converge to zero, i.e., $\Xi_i, \Psi_i \to 0$ as $i \to \infty$, provided that the auto-covariance function $K_{z\check{y}}(\tau)$ is bounded (i.e., exhibits no divergences).

$$\hat{K}_{z\check{y}}(\tau) = \frac{\Xi_0}{2} + \sum_{i=1}^{J} \Xi_i cos(i\omega_0\tau) + \sum_{i=1}^{J} \Psi_i sin(i\omega_0\tau), \quad \omega_0 = \frac{2\pi}{T}, \frac{-T}{2} \le \tau \le \frac{T}{2}. \tag{24}$$

Let T stand for the fundamental period of $K_{z\check{y}}(\tau)$. The finite Fourier cosine and sine coefficients are calculated according to equation (25).

$$\Xi_i = \frac{2}{T}\int_{-\frac{T}{2}}^{\frac{T}{2}} K_{z\check{y}}(\tau)cos(i\omega_0\tau)d\tau, \quad \Psi_i = \frac{2}{T}\int_{-\frac{T}{2}}^{\frac{T}{2}} K_{z\check{y}}(\tau)sin(i\omega_0\tau)d\tau, \quad i = 0,1,2,\cdots,J \tag{25}$$

After comparing (8) and (24), we can represent the vector components of $\alpha(t)$ and $\beta(t)$ as follows:

$$\alpha(t) = [\alpha_1(t) \quad \alpha_2(t) \quad \alpha_3(t) \quad \cdots \quad \alpha_{4J+1}(t)],$$
$$\beta(t) = [\beta_1(t) \quad \beta_2(t) \quad \beta_3(t) \quad \cdots \quad \beta_{4J+1}(t)],$$
$$\alpha_1(t) = \frac{\Xi_0}{2},$$
$$\alpha_i(t) = \Xi_{i-1}cos(\frac{2\pi(i-1)t}{T}), i = 2,3,\cdots,J+1,$$
$$\alpha_i(t) = \Xi_{i-(J+1)}sin(\frac{2\pi(i-(J+1))t}{T}), \quad i = J+2, J+3,\cdots,2J+1,$$
$$\beta_1(t) = 1,$$
$$\beta_i(t) = cos(\frac{2\pi(i-1)t}{T}), i = 2,3,\cdots,J+1,$$
$$\beta_i(t) = sin(\frac{2\pi(i-(J+1))t}{T}), i = J+2, J+3,\cdots,2J+1,$$
$$\alpha_i(t) = \Xi_{i-(2J+1)}sin(\frac{2\pi(i-(2J+1))t}{T}), \; i = 2J+2, 2J+3,\cdots,3J+1,$$
$$\alpha_i(t) = -\Xi_{i-(3J+1)}cos(\frac{2\pi(i-(3J+1))t}{T}), \; i = 3J+2, 3J+3,\cdots,4J+1,$$
$$\beta_i(t) = cos(\frac{2\pi(i-(2J+1))t}{T}), \; i = 2J+2, 2J+3,\cdots,3J+1$$
$$\beta_i(t) = sin(\frac{2\pi(i-(3J+1))t}{T}), \; i = 3J+2, 3J+3,\cdots,4J+1.$$

We can recursively compute the FL smoothing estimate $\hat{z}(t-Lag,t)$ of the signal $z(t-Lag)$ by substituting the functions $\check{A}(t)$, $\check{B}(t)$, $\alpha(t)$, and $\beta(t)$ into the robust RLS-FL smoothing algorithm of Theorem 1.

7 A Numerical Simulation Example

(26) represents a second-order mass-spring system governed by the state differential equation for the signal $z(t)$.

$$\begin{aligned} & y(t) = z(t) + v(t), z(t) = Hx(t), \\ & H = [1 \quad 0], \frac{dx(t)}{dt} = Ax(t) + \Gamma w(t), \\ & x(t) = \begin{bmatrix} x_1(t) \\ x_2(t) \end{bmatrix}, x(0) = \begin{bmatrix} 0.65 \\ 0.05 \end{bmatrix}, \\ & A = \begin{bmatrix} 0 & 1 \\ -\omega_n^2 & -2\zeta\omega_n \end{bmatrix}, \\ & \omega_n = \sqrt{3}, \zeta = \frac{2}{\omega_n}, \Gamma = \begin{bmatrix} 1 \\ -2 \end{bmatrix}, \\ & E[v(t)v(s)] = R\delta(t-s), \\ & E[w(t)w(s)] = Q\delta(t-s), Q = 1, \\ & E[v(t)w(s)] = 0, E[x(0)w(t)] \\ & \qquad = 0, E[x(0)v(t)] = 0 \end{aligned} \tag{26}$$

(27) presents the observation equation corresponding to the degraded signal $\check{z}(t)$, along with the state differential equation governing the evolution of the degraded state vector $\acute{x}(t)$.

$$\begin{aligned} & \check{y}(t) = \check{z}(t) + v(t), \check{z}(t) = \acute{H}(t)\acute{x}(t), \\ & \frac{d\acute{x}(t)}{dt} = \acute{A}(t)\acute{x}(t) + \Gamma w(t), \\ & \acute{A}(t) = A + \Delta A(t), \acute{H}(t) = H + \Delta H(t), \\ & \Delta A(t) = \begin{bmatrix} 0 & 0 \\ -0.1 * rand & -0.1 * rand \end{bmatrix}, \\ & \Delta H(t) = [0.1 \quad 0], E[\acute{x}(0)w(t)] \\ & \qquad = 0, E[\acute{x}(0)v(t)] = 0 \end{aligned} \tag{27}$$

The matrix $\Delta A(t)$ represents an additive uncertainty component to the nominal system matrix A. The variable rand provides a random scalar from a uniform distribution over the interval (0,1). The autocovariance function $K_{\check{z}}(\tau)$, representing the statistical dependence of the degraded signal $\check{z}(t)$ over time lag $\tau = t - s$, is approximated in (20) using a fifth-order polynomial expansion. Figure 1 shows the autocovariance function $K_{\check{z}}(\tau)$ of the degraded signal $\check{z}(t)$ and its fifth-order polynomial approximation $\hat{K}_{\check{z}}(\tau)$, both plotted against the time lag τ for $0 \le \tau \le 2.5$. This comparison highlights the accuracy and representational fidelity of the polynomial model in capturing the covariance structure of the degraded signal. The mean-square value (MSV) of the polynomial approximation errors for the autocovariance function $K_{\check{z}}(i\Delta)$ is computed using the formula $\frac{1}{2501}\sum_{i=0}^{2500}(K_{\check{z}}(i\Delta)-\hat{K}_{\check{z}}(i\Delta))^2$, where Δ=0.001. The resulting MSV is 1.38504×10^{-5}, indicating a high degree of accuracy in the fifth-order polynomial approximation of the autocovariance function over the interval. For $m=8$ in (21), the cross-covariance function $K_{z\check{y}}(\tau)$, representing the statistical relationship between the signal $z(t)$ and the observed value $\check{y}(s)$, is approximated using an eighth-order polynomial expansion. The resulting approximation, denoted $\hat{K}_{z\check{y}}(\tau)$, consists of $m+1=9$ terms. Figure 2 displays the cross-covariance function $K_{z\check{y}}(\tau)$, τ=t-s, between the signal $z(t)$ and the observed value $\check{y}(s)$, along with its polynomial approximation $\hat{K}_{z\check{y}}(\tau)$ constructed using $m=8$ and $M=45$. The functions are plotted over the interval $-2.5\le\tau\le2.5$, illustrating the accuracy of the polynomial representation in capturing the covariance structure across the specified lag domain. The MSV of the polynomial approximation errors for the cross-covariance function $K_{z\check{y}}(\tau)$ is computed using the formula $\frac{1}{5001}\sum_{i=-2500}^{2500}(K_{z\check{y}}(i\Delta)-\hat{K}_{z\check{y}}(i\Delta))^2$, where $\Delta=0.001$. The eighth-order polynomial yields an MSV of 3.12708×10^{-4} over $-2.5\le\tau\le2.5$, quantifying the approximation accuracy.

The components of $\check{A}(t)$ and $\check{B}(t)$ in the fifth-order polynomial approximation of $K_{\check{z}}(\tau)$ for $k=5$ and $K=21$ are given below:
$\check{A}_1(t)=-P_1$, $\check{A}_2(t)=5P_1t$, $\check{A}_3(t)=-10P_1t^2$, $\check{A}_4(t)=10P_1t^3$, $\check{A}_5(t)=-5P_1t^4$, $\check{A}_6(t)=P_1t^5$, $\check{A}_7(t)=P_2$, $\check{A}_8(t)=-4P_2t$, $\check{A}_9(t)=6P_2t^2$, $\check{A}_{10}(t)=-4P_2t^3$, $\check{A}_{11}(t)=P_2t^4$, $\check{A}_{12}(t)=-P_3$, $\check{A}_{13}(t)=3P_3t$, $\check{A}_{14}(t)=-3P_3t^2$, $\check{A}_{15}(t)=P_3t^3$, $\check{A}_{16}(t)=P_4$, $\check{A}_{17}(t)=-2P_4t$, $\check{A}_{18}(t)=P_4t^2$, $\check{A}_{19}(t)=-P_5$, $\check{A}_{20}(t)=P_5t$, $\check{A}_{21}(t)=P_6$, $\check{B}_1(t)=t^5$, $\check{B}_2(t)=t^4$, $\check{B}_3(t)=t^3$, $\check{B}_4(t)=t^2$, $\check{B}_5(t)=t$, $\check{B}_6(t)=1$, $\check{B}_7(t)=t^4$, $\check{B}_8(t)=t^3$, $\check{B}_9(t)=t^2$, $\check{B}_{10}(t)=t$, $\check{B}_{11}(t)=1$, $\check{B}_{12}(t)=t^3$, $\check{B}_{13}(t)=t^2$, $\check{B}_{14}(t)=t$, $\check{B}_{15}(t)=1$, $\check{B}_{16}(t)=t^2$, $\check{B}_{17}(t)=t$, $\check{B}_{18}(t)=1$, $\check{B}_{19}(t)=t$, $\check{B}_{20}(t)=1$, $\check{B}_{21}(t)=1$.

The $\alpha(t)$ and $\beta(t)$ components in the eighth-order polynomial approximation of $K_{z\check{y}}(\tau)$ for $m=8$ and $M=45$ are given by the following formulae:

$\alpha_1(t)=D_1$, $\alpha_2(t)=-8D_1t$, $\alpha_3(t)=28D_1t^2$, $\alpha_4(t)=-56D_1t^3$, $\alpha_5(t)=70D_1t^4$,
$\alpha_7(t)=28D_1t^6$, $\alpha_8(t)=-8D_1t^7$, $\alpha_9(t)=D_1t^8$,
$\alpha_{10}(t)=-D_2$, $\alpha_{11}(t)=7D_2t$, $\alpha_{12}(t)=-21D_2t^2$,
$\alpha_{13}(t)=35D_2t^3$, $\alpha_{14}(t)=-35D_2t^4$,
$\alpha_{15}(t)=21D_2t^5$, $\alpha_{16}(t)=-7D_2t^6$,
$\alpha_{17}(t)=D_2t^7$, $\alpha_{18}(t)=D_3$, $\alpha_{19}(t)=-6D_3t$,
$\alpha_{20}(t)=15D_3t^2$, $\alpha_{21}(t)=-20D_3t^3$,
$\alpha_{22}(t)=15D_3t^4$, $\alpha_{23}(t)=-6D_3t^5$,
$\alpha_{24}(t)=D_3t^6$, $\alpha_{25}(t)=-D_4$, $\alpha_{26}(t)=5D_4t$,
$\alpha_{27}(t)=-10D_4t^2$, $\alpha_{28}(t)=10D_4t^3$,
$\alpha_{29}(t)=-5D_4t^4$, $\alpha_{30}(t)=D_4t^5$, $\alpha_{31}(t)=D_5$,
$\alpha_{32}(t)=-4D_5t$, $\alpha_{33}(t)=6D_5t^2$,
$\alpha_{34}(t)=-4D_5t^3$, $\alpha_{35}(t)=D_5t^4$, $\alpha_{36}(t)=-D_6$,
$\alpha_{37}(t)=3D_6t$, $\alpha_{38}(t)=-3D_6t^2$, $\alpha_{39}(t)=D_6t^3$,
$\alpha_{40}(t)=D_7$, $\alpha_{41}(t)=-2D_7t$, $\alpha_{42}(t)=D_7t^2$,
$\alpha_{43}(t)=-D_8$, $\alpha_{44}(t)=D_8t$, $\alpha_{45}(t)=D_9$,
$\beta_1(t)=t^8$, $\beta_2(t)=t^7$, $\beta_3(t)=t^6$, $\beta_4(t)=t^5$, $\beta_5(t)=t^4$, $\beta_6(t)=t^3$, $\beta_7(t)=t^2$, $\beta_8(t)=t$, $\beta_9(t)=1$, $\beta_{10}(t)=t^7$, $\beta_{11}(t)=t^6$, $\beta_{12}(t)=t^5$, $\beta_{13}(t)=t^4$, $\beta_{14}(t)=t^3$, $\beta_{15}(t)=t^2$, $\beta_{16}(t)=t$, $\beta_{17}(t)=1$, $\beta_{18}(t)=t^6$, $\beta_{19}(t)=t^5$,
$\beta_{20}(t)=t^4$, $\beta_{21}(t)=t^3$, $\beta_{22}(t)=t^2$, $\beta_{23}(t)=t$, $\beta_{24}(t)=1$, $\beta_{25}(t)=t^5$, $\beta_{26}(t)=t^4$, $\beta_{27}(t)=t^3$, $\beta_{28}(t)=t^2$, $\beta_{29}(t)=t$, $\beta_{30}(t)=1$,
$\beta_{31}(t)=t^4$, $\beta_{32}(t)=t^3$, $\beta_{33}(t)=t^2$,
$\beta_{34}(t)=t$, $\beta_{35}(t)=1$, $\beta_{36}(t)=t^3$,
$\beta_{37}(t)=t^2$, $\beta_{38}(t)=t$, $\beta_{39}(t)=1$,
$\beta_{40}(t)=t^2$, $\beta_{41}(t)=t$, $\beta_{42}(t)=1$,
$\beta_{43}(t)=t$, $\beta_{44}(t)=1$, $\beta_{45}(t)=1$.

The script polyfit.m is used in MATLAB/Octave for curve fitting and computes the parameter sets P_i ($1\le i\le6$) and D_j ($1\le j\le9$). The FL smoothing estimates are computed recursively by substituting the autocovariance information $\check{A}(t)$ and $\check{B}(t)$ and the cross-covariance information $\alpha(t)$ and $\beta(t)$ into the robust RLS-FL smoothing algorithm of Theorem 1. Fig. 3 illustrates the signal $z(t)$ and the FL smoothing estimate $\hat{z}(t,t+0.005)$ vs. t for white Gaussian observation noise $N(0,0.1^2)$, assuming polynomial orders of $k=5$ and $m=8$. The MSV of the FL smoothing errors is 8.55712×10^{-3}. This is calculated using the formula: $\frac{1}{2500}\sum_{i=1}^{2500}(z(i\Delta)-\hat{z}(i\Delta,i\Delta+0.005))^2$, where Δ= 0.001. Figure 4 illustrates the mean-square values (MSVs) of the filtering and FL smoothing errors $z(t)-\hat{z}(t,t+Lag)$ vs. Lag, $0\le Lag\le0.005$ for the white Gaussian observation noises $N(0,0.1^2)$, $N(0,0.3^2)$, and $N(0,0.5^2)$, assuming polynomial orders of $k=5$ and $m=8$. Here, $\frac{1}{2500}\sum_{i=1}^{2500}(z(i\Delta)-\hat{z}(i\Delta,i\Delta+Lag))^2$, $0.001\le Lag\le0.005$, evaluates the MSVs of the FL smoothing errors. As seen from Fig. 4, for

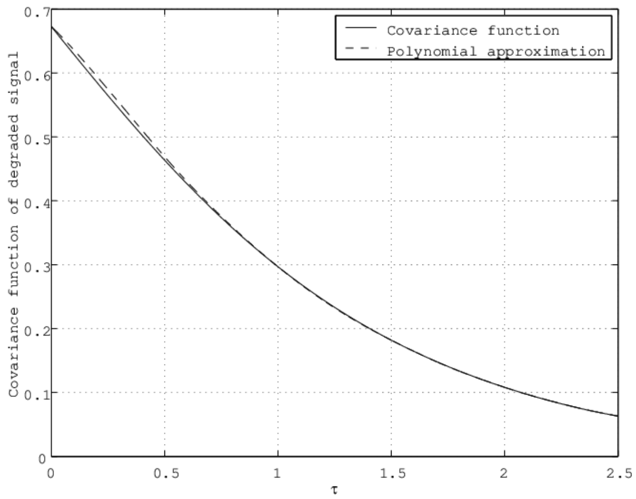

Fig. 1: Autocovariance function of the degraded signal $\breve{z}(t)$, $K_{\breve{z}}(\tau)$, and its fifth-order approximate polynomial function $\hat{K}_{\breve{z}}(\tau)$ vs. τ

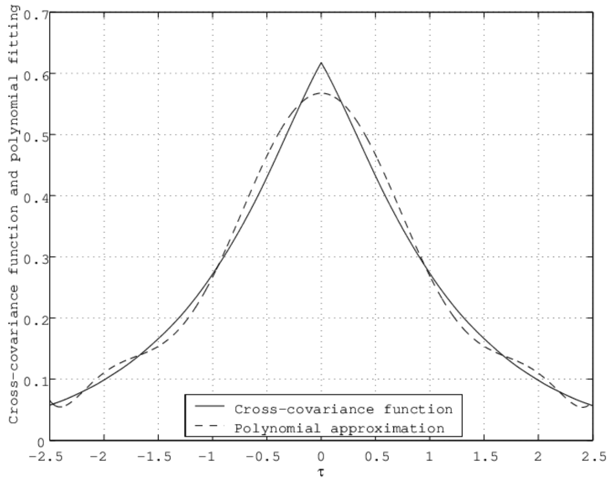

Fig. 2: Cross-covariance function $K_{z\breve{y}}(\tau)$, $\tau = t - s$, of the signal $z(t)$ with the observed value $\breve{y}(s)$ and its eighth-order approximate polynomial function $\hat{K}_{z\breve{y}}(\tau)$ vs. τ

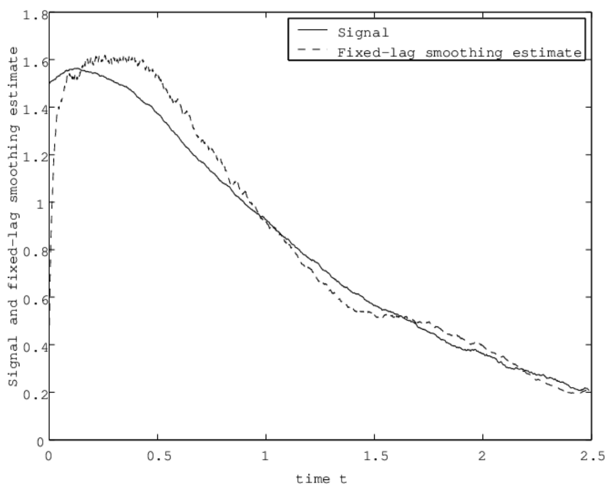

Fig. 3: Signal $z(t)$ ant FL smoothing estimate $\hat{z}(t, t + 0.005)$ vs. t for white Gaussian observation noise $N(0, 0.1^2)$, assuming polynomial orders of $k = 5$ and $m = 8$

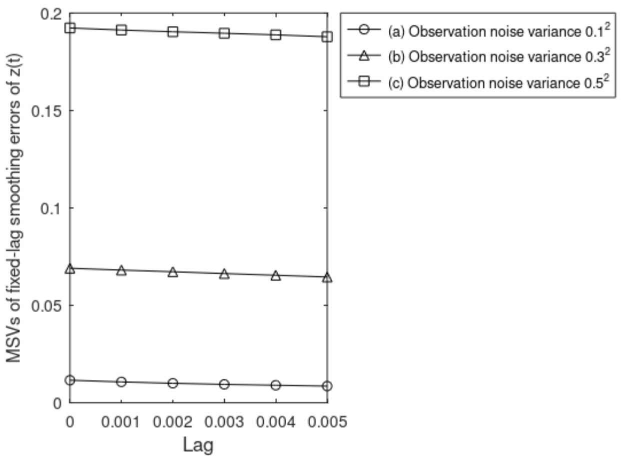

Fig. 4: Mean-square values of filtering and FL smoothing errors $z(t) - \hat{z}(t, t + Lag)$ vs. Lag, $0 \leq Lag \leq 0.005$, for the white Gaussian observation noises $N(0, 0.1^2)$, $N(0, 0.3^2)$, and $N(0, 0.5^2)$, assuming polynomial orders of $k = 5$ and $m = 8$

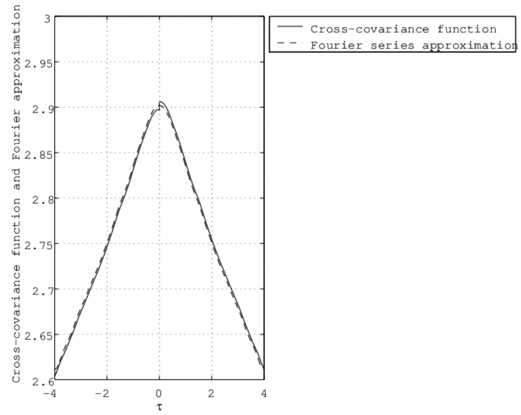

Fig. 5: Cross-covariance function $K_{z\breve{y}}(\tau)$, $\tau = t - s$, of the signal $z(t)$ with the observed value $\breve{y}(s)$ and its Fourier series approximation vs. τ for $J = 15$

each observation noise, the MSV of the FL smoothing error $(z(t) - \hat{z}(t, t + Lag))$ decreases as Lag increases ($0.001 \leq Lag \leq 0.005$). Figure 5 shows both the cross-covariance function $K_{z\breve{y}}(\tau), \tau = t - s$, between the signal $z(t)$ and the observation $\breve{y}(s)$, and the Fourier series approximation $\hat{K}_{z\breve{y}}(\tau)$ (τ) for $J = 15$ over the range $-4 \leq \tau \leq 4$. In Figure 5, the MSV of the Fourier series approximation errors for $K_{z\breve{y}}(i\Delta)$is evaluated as $\frac{1}{8001}\sum_{i=-4000}^{4000}(K_{z\breve{y}}(i\Delta) - \hat{K}_{z\breve{y}}(i\Delta))^2 = 1.69429 \times 10^{-5}$. Figure 6 presents the MSVs of the filtering and FL smoothing errors $z(t) - \hat{z}(t, t +$

Lag) as a function of Lag,

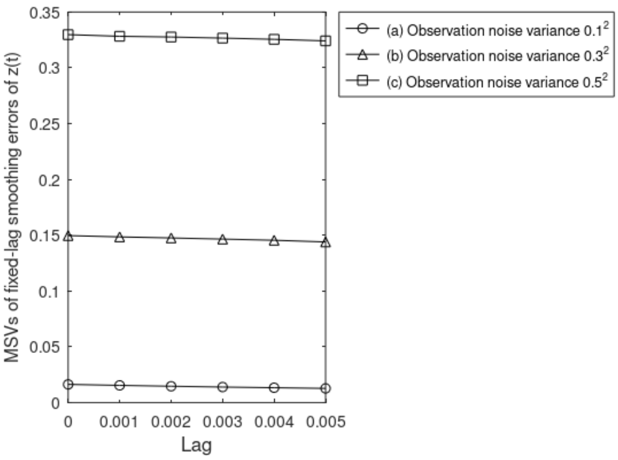

Fig. 6: Mean-square values of the filtering and FL smoothing errors $z(t) - \hat{z}(t, t + Lag)$ vs. Lag, $0 \leq Lag \leq 0.005$, for white Gaussian observation noises $N(0, 0.1^2)$, $N(0, 0.3^2)$, and $N(0, 0.5^2)$. The covariance information is approximated using Fourier series expansions, where the autocovariance function $\hat{K}_{\tilde{z}}(\tau)$ is represented by $N+1$ terms in (19) with $N = 15$, and the cross-covariance function $\hat{K}_{z\tilde{y}}(\tau)$ is represented by $2J + 1$ terms in (21) with $J = 15$

for $0 \leq Lag \leq 0.005$, under white Gaussian observation noises $N(0, 0.1^2)$, $N(0, 0.3^2)$, and $N(0, 0.5^2)$. Covariance information is approximated using Fourier series expansions: the autocovariance function $\hat{K}_{\tilde{z}}(\tau)$ is represented by N+1 terms in (19) with $N = 15$, and the cross-covariance function $\hat{K}_{z\tilde{y}}(\tau)$ is represented by $2J + 1$ terms in (21) with $J = 15$. For observation noises $N(0, 0.3^2)$ and $N(0, 0.5^2)$, the MSV of the FL smoothing errors $(z(t) - \hat{z}(t, t + Lag))$ decreases gradually as Lag increases ($0.001 \leq Lag \leq 0.005$). As shown in Figure 4 and Figure 6, the polynomial approximations consistently produce smaller MSVs of both filtering and FL smoothing errors than the Fourier series approximations, across all examined observation noises. Table 1 shows the MSVs of FL smoothing errors $z(t) - \hat{z}(t, t + Lag)$, $Lag = 0.005$, calculated using the least-squares FL smoother [16], the FL smoother using polynomial approximations ($k = 5$, $m = 8$), and the FL smoother using Fourier series approximations ($N = 15, J = 15$). Across all observation noise levels, the FL smoother based on the least squares method [16] consistently exhibits lower estimation accuracy than the two proposed FL smoothing approaches, which approximate covariance information using either Fourier series or polynomial representations. For all observation noise levels, the FL smoother that employs polynomial approximations of the covariance information achieves higher estimation accuracy than the FL smoother based on Fourier-series approximations.

Table 1: Mean square values (MSVs) of FL smoothing errors $z(t) - \hat{z}(t, t + Lag)$, $Lag = 0.005$, calculated using the lest-squares FL smoother [16], the FL smoother using polynomial approximations ($k = 5$, $m = 8$), and the FL smoother using Fourier series approximations ($N = 15, J = 15$)

Observation noise	MSVs of FL smoothing errors [16]	MSVs of FL smoothing errors calculated by the current polynomial approximation technique for $k = 5$ and $m = 8$	MSVs of FL smoothing errors calculated by the current Fourier series approximation technique for $N = 15$ and $J = 15$
$N(0, 0.1^2)$	2.30848×10^{-2}	8.55712×10^{-3}	1.27745×10^{-2}
$N(0, 0.3^2)$	2.63966×10^{-1}	6.45306×10^{-2}	1.44004×10^{-1}
$N(0, 0.5^2)$	5.34373×10^{-1}	1.87811×10^{-1}	3.24166×10^{-1}

8 Conclusion

This paper developed a robust suboptimal FL smoothing estimation method for uncertain, stochastic, linear, continuous-time systems. The underlying degraded state-space model incorporates uncertainty in the system matrices and observation vector. The robust RLS-FL smoothing algorithm, as presented in Theorem 1, enhances estimation accuracy by utilising covariance information. Specifically, the cross-covariance function between the signal and the observed values is approximated using either a polynomial expansion or a Fourier series. Similarly, the autocovariance function of the degraded signal can be expressed as a semi-degenerate function using either a polynomial or a Fourier series approximation. Derivation of a robust RLS-FL smoothing algorithm becomes analytically intractable when the cross-covariance function takes a semi-degenerate form. The proposed method overcomes this challenge by employing a degenerate kernel representation of the cross-covariance function between the signal and the degraded observations. This formulation simplifies the covariance structure, allowing for a tractable and computationally efficient implementation of the robust RLS-FL smoothing algorithm.

For all observation noise levels, the estimation accuracy of the FL smoother based on the least-squares method [16] is lower than that of the two proposed FL smoothing approaches, which approximate the covariance information using either Fourier-series or polynomial representations. Moreover, across all noise levels, the FL smoother employing polynomial approximations consistently achieves higher estimation accuracy than the Fourier-series-based FL smoother.

Numerical simulation results confirm the effectiveness of the proposed FL smoothing methods based on polynomial and Fourier-series approximations of the covariance information.

References:

[1] U. Lagerblad, H. Wentzel, A. Kulachenko, Study of a fixed-lag Kalman smoother for input and state estimation in vibrating structures, Inverse Problems in Science and Engineering, Vol. 9, 2021, pp. 1260–128. [Online]. Available: https://www.tandfonline.com/doi/full/10.1080/17415977.2020.1845669. (Accessed: January 18, 2026).

[2] S. Yi, M. Zorzi, Robust fixed-lag smoothing under model perturbations, Journal of the Franklin Institute, Vol. 360, 2023, pp. 458–483. [Online]. Available: https://www.sciencedirect.com/science/article/abs/pii/S0016003222007918. (Accessed: January 18, 2026).

[3] T.-C. Dong-Si, A. I. Mourikis, Motion tracking with fixed-lag smoothing: Algorithm and consistency analysis. Proc IEEE Int Conf Rob Autom., Shanghai, China, 2011, pp. 5655–5662. [Online]. Available: https://ieeexplore.ieee.org/document/5980267. (Accessed: January 18, 2026).

[4] B. Kwon, P. S. Kim, Novel unbiased optimal receding-horizon fixed-lag smoothers for linear discrete time-varying systems, Appl. Sci., Vo. 12, 2022, 7832. [Online]. Available: https://www.mdpi.com/2076-3417/12/15/7832. (Accessed: January 18, 2026).

[5] B. Chen, J. K. Tugnait, Interacting multiple model fixed-lag smoothing algorithm for Markovian switching systems, IEEE Transactions on Aerospace and Electronic Systems, Vol. 36, 2000, pp. 243–250. [Online]. Available: Interacting multiple model fixed-lag smoothing algorithm for Markovian switching systems | IEEE Journals & Magazine | IEEE Xplore. (Accessed: January 18, 2026).

[6] H. Wang, H. Zhang, G. Duan, H/sub /spl infin// fixed-lag smoothing for descriptor systems, Proceedings of the 2005, American Control Conference 2005, Portland, OR, USA, 2005, Vol. 4, 2005, pp. 2919–2924. [Online]. Available: H/sub /spl infin// fixed-lag smoothing for descriptor systems | IEEE Conference Publication | IEEE Xplore. (Accessed: January 18, 2026).

[7] K. Li, G. Zhou, L. Xu, Fixed-lag smoothing with linear equality constraints, 2017 20th International Conference on Information Fusion (Fusion), Xi'an, China, 2017, pp. 1–8. [Online]. Available: Fixed-lag smoothing with linear equality constraints | IEEE Conference Publication | IEEE Xplore. (Accessed: January 18, 2026).

[8] F. Papi, M. Bocquel, M. Podt, Y. Boers, Fixed-lag smoothing for bayes optimal knowledge exploitation in target tracking, IEEE Trans Signal Process., Vol. 62, 2014, pp. 3143–3152. [Online]. Available: Fixed-Lag Smoothing for Bayes Optimal Knowledge Exploitation in Target Tracking | IEEE Journals & Magazine | IEEE Xplore. (Accessed: January 18, 2026).

[9] S.-L. Sun, Distributed optimal component fusion weighted by scalars for fixed-lag Kalman smoother, Automatica, Vol. 41, 2005, pp. 2153–2159. [Online]. Available: https://www.sciencedirect.com/science/article/abs/pii/S0005109805002670. (Accessed: January 18, 2026).

[10] F. S. Cattivelli, A. H. Sayed, Diffusion strategies for distributed Kalman filtering and smoothing, IEEE Trans Autom Control, Vol. 55, 2010, 55, pp. 2069–2084. [Online]. Available: Diffusion Strategies for Distributed Kalman Filtering and Smoothing | IEEE Journals & Magazine | IEEE Xplore. (Accessed: January 18, 2026).

[11] B. Kwon, Z. Quan, S. Han, A robust fixed-lag receding horizon smoother for uncertain state space models, Int J Adapt Control Signal Process, Vol. 29, 2015, pp. 1354–1366. [Online]. Available: OASIS Repository@POSTECHLIBRARY: A robust fixed-lag receding horizon smoother for uncertain state space models. (Accessed: January 18, 2026).

[12] P. S. Kim, A computationally efficient fixed-lag smoother using recent finite

measurements, Measurement, Vol. 46, 2013, pp. 846–850. [Online]. Available: https://www.sciencedirect.com/science/article/abs/pii/S0263224112003703. (Accessed: January 18, 2026).

[13] H. Lee, S. Han, A continuous finite-time convergence fixed-lag FIR smoother using multiple IIR filters, J Franklin Inst., Vol. 359, 2022, pp. 5798–5826. [Online]. Available: https://www.sciencedirect.com/science/article/abs/pii/S0016003222003155. (Accessed: January 18, 2026).

[14] O. U. Rehman, I. R. Petersen, A robust continuous time fixed lag smoother for nonlinear uncertain systems, 52nd IEEE Conference on Decision and Control, Firenze, Italy, 2013, pp. 3750–3755. [Online]. Available: A robust continuous time fixed lag smoother for nonlinear uncertain systems | IEEE Conference Publication | IEEE Xplore (Accessed: January 18, 2026).

[15] A. Al-Hagri, L. Caglio, H. Stang, E. Katsanos, Application of fixed-lag Kalman smoother for nonlinear state estimation, J. Phys.: Conf. Series, 2647, 2024, 182034. [Online]. Available: https://iopscience.iop.org/article/10.1088/1742-6596/2647/18/182034. (Accessed: January 18, 2026).

[16] S. Nakamori, Design of recursive least-squares fixed-lag smoother using covariance information in linear continuous stochastic systems, Applied Mathematical Modelling, Vol. 31, 2007, pp. 1609-1620. [Online]. Available: https://www.sciencedirect.com/science/article/pii/S0307904X06001193. (Accessed: January 18, 2026).

[17] R. Bellman, S. Ueno, Invariant imbedding and the resolvent of Fredholm integral equations with semi-degenerate kernels, Journal of Mathematical Analysis and Applications, Vol. 44, 1973, pp. 264-273. [Online]. Available: https://www.sciencedirect.com/science/article/pii/0022247X73900425. (Accessed: January 18, 2026).

[18] L. V. Fausett, Applied Numerical Analysis Using MATLAB, Pearson Prentice Hall, Upper Saddle River, NJ, USA, 2008. [Online]. Available: https://books.google.co.jp/books/about/Applied_Numerical_Analysis_Using_MATLAB.html?id=15CfQAAACAAJ&redir_esc=y. (Accessed: January 18, 2026).

[19] S. Boyd, Lecture 6 Least-squares application. [Online]. Available: https://see.stanford.edu/materials/lsoeldsee263/06-ls-app.pdf. (Accessed: January 18, 2026).

[20] W. K. Nicholson, Best Approximation and Least Squares, LibreTexts Mathematics. [Online]. Available: https://math.libretexts.org/Bookshelves/Linear_Algebra/Linear_Algebra_with_Applications_(Nicholson)/05%3A_Vector_Space_R/5.06%3A_Best_Approximation_and_Least_Squares. (Accessed: January 18, 2026).

[21] R. L. Burden, J. D. Faires, A. M. Burden, Numerical Analysis, 10th ed., Engage Learning: Australia, Brazil, Mexico, Singapore, United Kingdom, United States , 2015. [Online]. Available: https://www.amazon.com/Numerical-Analysis-Richard-L-Burden/dp/1305253663. (Accessed: January 18, 2026).

APPENDIX

From (7) and (8), $K_{z\breve{y}}(t-Lag,s)=\alpha(t-Lag)\beta^T(s)$ is valid. Taking into this relationship and introducing an integral equation

$$J(t,s)R=\beta^T(s)-\int_0^t J(t,s')K_{\breve{z}}(s',s)ds', \tag{A-1}$$

$h(t,s)$is given by (A-2).

$$h(t,s)=\alpha(t-Lag)J(t,s) \tag{A-2}$$

Differentiating (A-1) with respect to t, we have (A-3).

$$\frac{\partial J(t,s)}{\partial t}R=-J(t,t)K_{\breve{z}}(t,s)-\int_0^t \frac{\partial J(t,s')}{\partial t}K_{\breve{z}}(s',s)ds' \tag{A-3}$$

From (9), the autocovariance function of the degraded signal is expressed as $\breve{K}(t,s)=\breve{A}(t)\breve{B}^T(s), 0\le s\le t$. Taking this relationship into account and introducing

$$J_1(t,s)R=\breve{B}^T(s)-\int_0^t J_1(t,s')K_{\breve{z}}(s',s)ds', \tag{A-4}$$

$\frac{\partial J(t,s)}{\partial t}$is given by (A-5).

$$\frac{\partial J(t,s)}{\partial t}=-J(t,t)\breve{A}(t)J_1(t,s) \tag{A-5}$$

Introducing

$$r(t)=\int_0^t J(t,s')\breve{B}(s')ds', \tag{A-6}$$

from (9), $J(t,t)$ satisfies (A-7).

$$J(t,t)R=\beta^T(t)-r(t)\breve{A}^T(t) \tag{A-7}$$

Differentiating $r(t)$ with respect to t, from (A-5), we have (A-8).

$$\begin{aligned}\frac{dr(t)}{dt}&=J(t,t)\breve{B}(t)+\int_0^t \frac{\partial J(t,s')}{\partial t}\breve{B}(s')ds'\\&=J(t,t)\breve{B}(t)-J(t,t)\breve{A}(t)\int_0^t J_1(t,s')\breve{B}(s')ds'\end{aligned} \tag{A-8}$$

Introducing a function

$$r_1(t)=\int_0^t J_1(t,s')\breve{B}(s')ds', \tag{A-9}$$

we obtain (A-10).

$$\begin{aligned}&\frac{dr(t)}{dt}=J(t,t)(\breve{B}(t)-\breve{A}(t)r_1(t)),\\&r(0)=0\end{aligned} \tag{A-10}$$

Noting that $K_{\breve{z}}=\breve{B}(t)\breve{A}^T(s)$ is valid for $0\le s\le t$, from (9), and using (A-4) and (A-9), $J_1(t,t)$ satisfies (A-11).

$$\begin{aligned}J_1(t,t)R&=\breve{B}^T(t)-\int_0^t J_1(t,s')K_{\breve{z}}(s',t)ds'\\&=\breve{B}^T(t)-\int_0^t J_1(t,s')\breve{B}(s')ds'\breve{A}^T(t)\\&=\breve{B}^T(t)-r_1(t)\breve{A}^T(t)\end{aligned} \tag{A-11}$$

Differentiating (A-4) with respect to t yields (A-12).

$$\frac{\partial J_1(t,s)}{\partial t}R = -J_1(t,t)\check{K}(t,s) - \int_0^t \frac{\partial J_1(t,s')}{\partial t}K_{\check{z}}(s',s)ds' \tag{A-12}$$

From (9) and (A-4), $\frac{\partial J_1(t,s)}{\partial t}$ is given by (A-13).

$$\frac{\partial J_1(t,s)}{\partial t} = -J_1(t,t)\check{A}(t)J_1(t,s) \tag{A-13}$$

Differentiating (A-9) with respect to t, from (A-9) and (A-13), we obtain (A-14).

$$\begin{aligned}\frac{dr_1(t)}{dt} &= J_1(t,t)\check{B}(t) + \int_0^t \frac{\partial J_1(t,s')}{\partial t}\check{B}(s')ds' \\ &= J_1(t,t)\check{B}(t) - J_1(t,t)\check{A}(t)\int_0^t J_1(t,s')\check{B}(s')ds'\, J_1(t,t)\left(\check{B}(t) - \check{A}(t)r_1(t)\right), \\ r_1(0) &= 0\end{aligned} \tag{A-14}$$

The FL smoothing estimate $\hat{z}(t-D,t)$ of $z(t-D)$ is given by (3). Substituting (A-2) into (3) yields (A-15).

$$\hat{z}(t-D,t) = \alpha(t-Lag)\int_0^t J(t,s')\check{y}(s')ds' \tag{A-15}$$

Introducing

$$e(t) = \int_0^t J(t,s')\check{y}(s')ds', \tag{A-16}$$

we obtain (A-17).

$$\hat{z}(t-D,t) = \alpha(t-Lag)e(t) \tag{A-17}$$

Differentiating (A-16) with respect to t, from (A-5), we obtain (A-18).

$$\begin{aligned}\frac{de(t)}{dt} &= J(t,t)\check{y}(t) - J(t,t)\check{A}(t)\int_0^t J_1(t,s')\check{y}(s')ds' \\ &= J(t,t)(\check{y}(t) - \check{A}(t)e_1(t)), \\ e(0) &= 0\end{aligned} \tag{A-18}$$

Here, $e_1(t)$ is given by (A-19).

$$e_1(t) = \int_0^t J_1(t,s')\check{y}(s')ds' \tag{A-19}$$

Differentiating (A-19) with respect to t, from (A-13), we obtain (A-20).

$$\begin{aligned}\frac{de_1(t)}{dt} &= J_1(t,t)\check{y}(t) - J_1(t,t)\check{A}(t)\int_0^t J_1(t,s)\check{y}(s')ds' \\ &= J_1(t,t)(\check{y}(t) - \check{A}(t)e_1(t)), \\ e_1(0) &= 0\end{aligned} \tag{A-20}$$

(Q.E.D.)

Contribution of Individual Authors to the Creation of a Scientific Article (Ghostwriting Policy)
The author contributed to the present research, at all stages from the formulation of the problem to the final findings and solution.

Sources of Funding for Research Presented in a Scientific Article or Scientific Article Itself
No funding was received for conducting this study.

Conflict of Interest
The authors have no conflicts of interest to declare.